Taylor & Francis
Taylor & Francis Group

Journal of Toxicology and Environmental Health, Part A
Current Issues

ISSN: 1528-7394 (Print) 1087-2620 (Online) Journal homepage: https://www.tandfonline.com/loi/uteh20

Mouse pulmonary response to dust from sawing Corian®, a solid-surface composite material

W. Kyle Mandler, Chaolong Qi, Marlene S. Orandle, Khachatur Sarkisian, Robert R. Mercer, Aleksandr B. Stefaniak, Alycia K. Knepp, Lauren N. Bowers, Lori A. Battelli, Justine Shaffer, Sherri A. Friend, Yong Qian & Jennifer D. Sisler

To cite this article: W. Kyle Mandler, Chaolong Qi, Marlene S. Orandle, Khachatur Sarkisian, Robert R. Mercer, Aleksandr B. Stefaniak, Alycia K. Knepp, Lauren N. Bowers, Lori A. Battelli, Justine Shaffer, Sherri A. Friend, Yong Qian & Jennifer D. Sisler (2019) Mouse pulmonary response to dust from sawing Corian®, a solid-surface composite material, Journal of Toxicology and Environmental Health, Part A, 82:11, 645-663, DOI: 10.1080/15287394.2019.1640816

To link to this article: https://doi.org/10.1080/15287394.2019.1640816

JOURNAL OF TOXICOLOGY AND ENVIRONMENTAL HEALTH, PART A
2019, VOL. 82, NO. 11, 645–663
https://doi.org/10.1080/15287394.2019.1640816

Taylor & Francis
Taylor & Francis Group

Mouse pulmonary response to dust from sawing Corian®, a solid-surface composite material

W. Kyle Mandler[a], Chaolong Qi[b], Marlene S. Orandle[a], Khachatur Sarkisian[a], Robert R. Mercer[a], Aleksandr B. Stefaniak[c], Alycia K. Knepp[c], Lauren N. Bowers[c], Lori A. Battelli[a], Justine Shaffer[a], Sherri A. Friend[a], Yong Qian[a], and Jennifer D. Sisler[a]

[a]Health Effects Laboratory Division, National Institute for Occupational Safety and Health, Morgantown, WV, USA; [b]Division of Applied Research, National Institute for Occupational Safety and Health, Cincinnati, OH, USA; [c]Respiratory Health Division, National Institute for Occupational Safety and Health, Morgantown, WV, USA

ABSTRACT

Corian®, a solid-surface composite (SSC), is composed of alumina trihydrate and acrylic polymer. The aim of the present study was to examine the pulmonary toxicity attributed to exposure to SSC sawing dust. Male mice were exposed to either phosphate buffer saline (PBS, control), 62.5, 125, 250, 500, or 1000 µg of SSC dust, or 1000 µg silica (positive control) *via* oropharyngeal aspiration. Body weights were measured for the duration of the study. Bronchoalveolar lavage fluid (BALF) and tissues were collected for analysis at 1 and 14 days post-exposure. Enhanced-darkfield and histopathologic analysis was performed to assess particle distribution and inflammatory responses. BALF cells and inflammatory cytokines were measured. The geometric mean diameter of SSC sawing dust following suspension in PBS was 1.25 µm. BALF analysis indicated that lactate dehydrogenase (LDH) activity, inflammatory cells, and pro-inflammatory cytokines were significantly elevated in the 500 and 1000 µg SSC exposure groups at days 1 and 14, suggesting that exposure to these concentrations of SSC induced inflammatory responses, in some cases to a greater degree than the silica positive control. Histopathology indicated the presence of acute alveolitis at all doses at day 1, which was largely resolved by day 14. Alveolar particle deposition and granulomatous mass formation were observed in all exposure groups at day 14. The SSC particles were poorly cleared, with 81% remaining at the end of the observation period. These findings demonstrate that SSC sawing dust exposure induces pulmonary inflammation and damage that warrants further investigation.

Abbreviations: ANOVA: Analysis of Variance; ATH: Alumina Trihydrate; BALF: Bronchoalveolar Lavage Fluid; D_{pg}: Geometric Mean Diameter; FE-SEM: Field Emission Scanning Electron Microscopy; IACUC: Institutional Animal Care and Use Committee; IFN-γ: Interferon Gamma; IL-1 B: Interleukin-1 Beta; IL-10: Interleukin-10; IL-12: Interleukin-12; IL-2: Interleukin-2; IL-4: Interleukin-4; IL-5: Interleukin-5; IL-6: Interleukin-6; KC/GRO: Neutrophil-Activating Protein 3; MMAD: Mass Median Aerodynamic Diameter; PBS: Phosphate-Buffered Saline; PEL: Permissible Exposure Limit; PM: Polymorphonuclear Leukocytes; PNOR: Particles Not Otherwise Regulated; SEM/EDX: Scanning Electron Microscope/Energy-Dispersive X-Ray; SSA: Specific Surface Area; SSC: Solid Surface Composite; TNFα: Tumor Necrosis Factor-Alpha; VOC: Volatile Organic Compounds; σ_g: Geometric Standard Deviation.

KEYWORDS

Particle toxicity; composites; pulmonary injury; airborne particles; risk assessment

Introduction

Corian®, a solid-surface composite (SSC), is a material commonly used in countertops and sink basins, but also in furniture, art installations, decorative lighting, and building cladding and is composed of a proprietary blend of powdered alumina trihydrate ($Al(OH)_3$, ATH), acrylic polymer, and other bindings or colorants (Corian Solid Surface Product Overview 2018). Alumina trihydrate is a purified form of the aluminum-rich ore, bauxite, and commonly used in this raw form as a fire-retardant. SSC is cut into sheet goods by the manufacturer, and then transported to fabricators for installation. Working with SCC during the manufacturing process and installation such as sawing and sanding generates large amounts of airborne contaminants including mixed-composition

CONTACT Yong Qian yaq2@cdc.gov Health Effects Laboratory Division, National Institute for Occupational Safety and Health, 1095 Willowdale Road, Morgantown, WV 26505, USA

Color versions of one or more of the figures in the article can be found online at www.tandfonline.com/uteh.
Supplemental data can be accessed here.

particles and volatile organic compounds (VOCs) may be released (Qi, Echt, and Murata 2016).

Human exposure to metal particulate matter (PM), including aluminum (Al), has been associated with pulmonary inflammation (Schwarz et al. 1998), alveolar proteinosis (Chew, Nigam, and Sivakumaran 2016) and acute lung injury (Ghio, Carraway, and Madden 2012). ATH, the principal component of SSC, demonstrated a fibrotic potential in the rat lung (Stacy et al. 1959). In addition, manufacturing and fabricating products containing plastic containing acrylate polymers release ultrafine particles and VOCs (Unwin et al. 2013).

Little information is available regarding the toxicity of Corian® dust in humans. Raghu et al. (2014) reported a case of fatal pulmonary fibrosis in a worker who sawed, ground, machine-drilled, and sanded Corian® for 16 years. This case was associated with deposition of particles containing Al in the lungs. McKeever, Okaneku, and LaSala (2014) noted that sandpapers containing aluminum oxide used by the patient may have been the source of Al detected in the lungs, and that the presence of other dust and PM in the workplace acts as confounding factors, precluding the ability to assign the blame of the observed toxicity to Corian® (Gannon and Rickard 2014).

The nature of the particles generated from SSC and their combination with other airborne contaminants are not well understood and the toxicological consequences remain to be determined. A preliminary study in an automatic lab setting revealed that 31.8% of the total airborne dust mass from sawing Corian® was respirable (Qi, Echt, and Murata 2016). The same study also found that respirable particles contained approximately 82% ATH. (Qi, Echt, and Murata 2016) also demonstrated that all detected Al originated from the SSC material, as no Al was contained in the saw blade and no sandpaper was used. The number-based aerodynamic size distribution exhibited a geometric mean diameter, (d_{pg}), of 1.05 μm and an average total concentration of 871.9 particles/cm^3, while the ultrafine portion of the airborne particles contained d_{pg} at 11.8 nm and an average total concentration of 1.19×10^6 particles/cm^3. The large amount of ultrafine particles produced during SSC sawing is particularly concerning, as inhaled ultrafine particles were demonstrated to produce greater pulmonary effects than larger particles per given mass. (Chang, Chen, and Yang 2015; Huang et al. 2011; Oberdorster 2001).

The ATH content and a large number of ultrafine particles released by SSC sawing suggest that exposure to these SSC dusts may pose a risk for deleterious pulmonary effects, including inflammation and pulmonary fibrosis. At present, there have been no apparent systematic investigations of the pulmonary toxicity elicited by the mixture of ingredients composing SSC. Therefore, the objective of this study was to evaluate the acute pulmonary response from exposure to SSC sawing dusts, whose Al content may be attributed to the SSC material alone, in a murine model for up to 14 days post-exposure following oropharyngeal aspiration of the airborne dust.

Methods

Particle generation

Particles were generated and collected in the manner as reported by Qi, Echt, and Murata (2016). For additional details, please refer to Supplemental file 1.

Material characterization

Hydrodynamic diameter and zeta potential were determined using dynamic light scattering and laser Doppler electrophoresis, respectively (Zetasizer Nano ZS90, Malvern Instruments Ltd., Malvern, UK). The samples were prepared by suspending SSC dust in 10 mM NaCl. The suspension was sonicated in three 20-sec intervals, with 10-sec pauses after each 20-sec sonication, for a total sonication time of 60 sec. Surface area of SSC dust was determined using nitrogen gas adsorption (ASAP 2020, Micrometrics Instrument Corporation, Norcross, GA). Samples were prepared by adding SSC dust to a pre-weighed sample tube and degassed under light vacuum at 300°C for 2 h then allowed to cool. A value of 1.62×10^{-19} m^2 was employed for the molecular cross-sectional area of N_2 at 77 K and surface area was

calculated from at least five adsorption points in the range p/p° = 0.01 to 0.3 and normalized to dry sample mass to obtain specific surface area (SSA) with units of m^2/g.

The morphology and size of SSC particles were determined utilizing field emission scanning electron microscopy (FE-SEM). A 0.1% (w/w) suspension of particles using saline was prepared and sonicated for 3 min (energy delivered = 1000 J). The final concentration was 0.02% (w/w) and 1 ml was passed through a 0.2 μm polycarbonate filter (Steriltech Corp., Kent, WA). A section from each filter was imaged at 2 K magnification using 5 kV accelerating voltage (Hitachi S-4800, Hitachi High Technologies America, Inc., Dallas, TX). Ten fields of view were randomly selected for imaging, capturing a total of 340 particles, the diameters of which were measured manually using ImageJ software (National Institutes of Health, Bethesda, MD). In addition, the Al content of the dusts collected from the Teflon® filter cartridges was analyzed following NIOSH Method 7303 (NIOSH 2003), which uses inductively coupled plasma (ICP).

Animals

Eight-week old male, pathogen-free, C57BL/6J mice weighing 22.6 ± 0.3 g were obtained from Jackson Laboratories (Bar Harbor, ME). Mice were housed individually and allowed to acclimate for 1 week in an AAALAC international-accredited animal facility. Immediately after exposure, 4 h after exposure, and daily thereafter, animal weight was monitored to assess the health of the animals. All procedures performed on animals were approved by the NIOSH Institutional Animal Care and Use Committee (IACUC).

Mice were assigned to exposure groups using a randomized complete block design. Because bronchoalveolar lavage fluid (BALF) interferes with accurate histopathology assessment, two groups of animals for each time point (1 and 14 days post-exposure) were used for each dose (Table 2 for specific n values per group). Mice were exposed to either a saline (PBS) vehicle control, 62.5, 125, 250, 500 or 1000 μg SSC dust, or 1000 μg silica (Min-USil-5, US Silica, Berkeley Springs, WV) as a positive control utilizing oropharyngeal aspiration as previously described by Mercer et al. (2011). Briefly, mice were anesthetized using isoflurane. Once lightly anesthetized, the animals were positioned vertically on a slant board. The mouths were opened, the tongues restrained and moved to expose the oral cavities. Particle samples suspended in 50 μl PBS were placed at the base of the tongue and the animals were restrained until they took two full breaths (but for not longer than 15 sec). Once the mice were dosed, animals were removed from the slant board and placed on its left side to fully recover. The mice were monitored immediately, 1 and 8 h after dosing for full recovery from anesthesia. Mice were given wellness checks and weighed daily to monitor the health of animals. In these examinations, animals are checked to ensure animals were active and alert, as well as eating and drinking based upon the presence of feces and urine in the bedding. At 1 or 14 days post-exposure, animals were administered an overdose of sodium pentobarbital (>100 mg/kg body weight) (Fatal Plus, Vortech Pharmaceuticals Ltd., Dearborn, MI) *via* intraperitoneal (IP) injection followed by exsanguination. Mice were used to determine whole lung Al deposition immediately post-exposure, lung clearance, inflammatory and damage markers in BALF, or histopathologic responses.

Mouse pulmonary exposure calculations

Several estimations and assumptions were made in order to determine the relationship between murine model dosages and human exposure time. First, for a human worker, an exposure to an SSC aerosol of 2.5 mg/m^3–50% of the OSHA Permissible Exposure Limit (PEL) for Particles Not Otherwise Regulated (PNOR) – was assumed. The measured SSC dust mass median aerodynamic diameter (MMAD) was 1.6 μm, resulting in an estimated 10% alveolar deposition fraction (Phalen 1984), the minute ventilation of a worker performing light duties is 20 L/min (0.02 m^3/min) (Galer et al. 1992), and average human alveolar epithelium surface area is 102 m^2 (Stone et al. 1992). Finally, it was assumed that a worker would be exposed for 4 h shifts, 5 days per week, for 50 weeks per year. Thus, exposure levels used

in this study of 62.5, 125, 250, 500, and 1000 µg correlate with a cumulative human alveolar deposition, in the absence of clearance, resulting from working with SSC for 0.44, 0.84, 1.7, 3.4, and 6.8 years, respectively (Equations 1–4).

*Eq. 1. Exposure rate = Minute ventilation * Permissible Exposure Limit * Deposition fraction*

$$\frac{0.005\ mg}{min} = \frac{0.02\ m^3}{\text{min}} * \frac{2.5\ mg}{m^3} * 10\%$$

*Eq. 2. Yearly deposition = Exposure rate * Exposure duration*

$$\frac{300\ mg}{year} = \frac{0.005\ mg}{min} * \frac{60\ min}{hour} * \frac{4\ hrs}{day} * \frac{5\ days}{week} * \frac{50\ weeks}{year}$$

Eq. 3. Exposure relative to alveolar surface area = Yearly deposition/human alveolar surface area

$$\frac{2.94\ \text{mg}/m^2}{\text{year}} = \frac{300\ mg}{102 m^2}$$

Eq. 4. Mouse alveolar surface area/exposure relative to alveolar surface area = Human equivalent exposure years

$$\frac{Aspiration\ Dose\ (mg)}{0.05 m^2} \Big/ \frac{2.94\ \text{mg}/m^2}{\text{year}} = Human\ equivalent\ exposure\ years$$

Bronchoalveolar lavage fluid (BALF)

The post-exposure times of 1 day and 14 days were selected to determine if acute lung damage and inflammation resolved or were persistent as determined by markers in BALF samples as described previously by Mercer et al. (2013). Bronchoalveolar lavage of the whole lung was performed by inserting a cannula into the trachea and gently flushing with Ca^{2+} and Mg^{2+} free phosphate-buffered saline (PBS), pH 7.4 with addition of 0.55 mM D-glucose. The initial whole lung lavage was performed twice using 0.6 ml PBS for a collection volume of 1.2 ml, which was processed for cytokine and lactate dehydrogenase (LDH) activity analysis. Four subsequent lavages were performed using a 1 ml aliquot per lavage for a collection volume of 4 ml, which was utilized for cell differential quantification. BALF cells were collected through centrifugation (1,500 × g, 5 min, 4°C) of the first and subsequent lavages, cell pellets were combined, washed with 1 ml PBS, and centrifuged (1,500 × g, 5 min, 4°C). BALF cells were re-suspended with 250 µL PBS and total cell counts were determined using a Coulter Counter (Multisizer 4, Beckman Coulter, Brea CA). Cytospins of the BALF cells were generated using a Shandon Cytospin 4 (Thermo Fisher; Waltham, MA) and stained with modified Wright stain (Thermo Fisher). Cytospins were analyzed for cell differentials using an Olympus AX70 light microscope (Tokyo, Japan) coupled with Olympus DP73 camera, and analyzed using the Olympus CellSens Dimension program. Two-hundred cells per slide were counted. BALF was analyzed for LDH activity, a measure of cytotoxicity, using a COBAS MIRA Plus (Roche Diagnostic Systems, Montclair, NJ) as previously described (Mercer et al. 2013). Fresh samples were assayed via manufacturer's protocol where the chemical oxidation of lactate to pyruvate coupled with the reduction of NAD+ was measured at 340 nm.

Enhanced-darkfield light microscopy imaging of SSC particles

SSC particles in sections from exposed lungs were assessed utilizing an enhanced-darkfield optical system (described below). These particles scatter light to a greater degree than the surrounding tissues due to a difference in refractive index and more crystalline order of particles in the SSC. The enhanced-darkfield optical system images light scattered in the section and, thus, particles in the section stand-out from the surrounding tissues with high contrast. This method of imaging may be used to scan lung sections at relatively low magnification to identify nanoparticles that might not be detected by other optical means (Ma et al. 2015; McKinney et al. 2012; Mercer et al. 2013, 2017). Typically, the image intensity of particles in tissue sections is approximately 20-fold that of the embedded tissue (Mercer et al. 2017).

Sections for dark-field examination were cut from paraffin blocks at 5-micron thickness and collected on ultrasonically cleaned, laser cut slides (Schott North America Inc., Elmsford, N.Y. 10523) to avoid

contamination from the ground edges of traditional slides. After staining with Sirius Red-Hematoxylin, slides were dehydrated in xylene and coverslipped with Permount (Fisher Scientific Co., Pittsburgh, PA) containing 5% xylene by volume. Just before mounting, the xylene-Permount was centrifuged at 10,000 x g for 10 min to remove contaminating particles.

The optical microscopes consist of a transmitted light microscope (Olympus BX63 with motorized condenser, controller and reflected light system) and a CytoViva enhanced darkfield microscope (EDM) (CytoViva, Auburn, AL 36830). The CytoViva EDM has a high signal-to-noise, dark-field illumination optical system that is adapted to an Olympus BX41 microscope which also includes a hyperspectral imaging camera with ENVI 4.8 analysis software and the CytoViva 3-D positioning and analysis software for serial section reconstruction. Both transmission light microscope and EDM were equipped with an Olympus DP73 digital camera with CellSens Dimension camera control and measurement software (Olympus America Inc., Center Valley, PA 18034). Images for the transmission light microscope and EMD systems were captured at 4800 × 3600 pixels or 2400 × 1800 pixels, respectively.

Determination of high dose SSC particle clearance from the lungs

Morphometry of SSC particles in lung sections at 1 and 14 days after exposure was used to measure the clearance of particles from the lungs. To make these measurements, 10 to 12 enhanced-darkfield light microscopy images were taken uniformly across longitudinal cross-sections of the left lung with a 60x objective. In order to analyze alveolar region clearance, micrographs containing airways or blood vessels larger than 25 microns were excluded from the series. The area of SSC particles to alveolar region area was then determined for the series of images using image intensity to detect the SSC particles with the threshold and particle detection features of ImageJ. This process was easily accomplished, as the typical image intensity of SSC particles was 240 to 250 on a 0 to 255 scale while the image intensity of tissues ranged from 15 to 50. Two such series of images were taken, analyzed and averaged for each animal with four animals examined at day 1, and 5 animals at day 5. The % SSC particle clearance was then determined from % SSC particle area at day 14 to that at day 1 post-exposure.

Histopathological analysis

Groups of mice (n = 8), separate from the animals used for BAL and cytokine analysis, were exposed by oropharyngeal aspiration to three doses of SSC dust (1 mg = high, 250 μg = intermediate and 62.5 μg = low), and sacrificed at days 1 and 14 post-exposure. Two animals from the 14 day 1000 μg SSC group exhibited a greater than 20% reduction in the first two days from their pre-exposure body weight and were removed from the study for welfare considerations before completion, resulting in an n = 6 for that group. These time points provide histopathological information concerning acute particle-induced inflammation. At necropsy, the left lung was inflated with 0.5 ml 10% neutral buffered formalin. The right lungs were tied off to be employed for other analyses. Sections of the lung were fixed, embedded in paraffin, sectioned at 5 microns, and stained with hematoxylin and eosin (H&E) for evaluation of routine histopathology. A board-certified veterinary pathologist at NIOSH (Morgantown, WV) performed all histopathologic analysis. The severity of lung pathology was scored using the following criteria: 1 = minimal, 2 = mild, 3 = moderate, and 4 = severe changes. Further details regarding these scores were previously published (Mann et al. 2012; Shackelford et al. 2002). Mean lung pathology scores and incidence for each group are summarized in Table 1.

Table 1. Number of animals affected and mean lung pathology score (parentheses). The severity of lung pathology was scored using the following criteria: 1 = minimal changes, 2 = mild changes, 3 = moderate changes, and 4 = severe changes. Two mice in the high exposure group were euthanized before the end of the study for animal health and welfare concerns.

	High (1mg)	Intermediate (250 μg)	Low (62.5 μg)
SSC exposure	n = 6	n = 8	n = 8
Day 1	6 (2.5 ± 0.8)	8 (2.5 ± 0.5)	8 (1.5 ± 0.5)
Day 14	6 (2.7 0.8)	6 (1 ± 0)	2 (1 ± 0)

Table 2. Number of animals in the lavage group used for each time point and SSC dose.

SSC exposure (μg)	Control	62.5	125	250	500	1000
Day 1 (n)	10	8	8	7	7	8
Day 14 (n)	10	8	8	8	8	8

For elemental analysis, sections of the lung were cut at 8 microns and placed on carbon planchets. The sections were evaluated using a Bruker scanning electron microscope/energy-dispersive X-ray (SEM/EDX) (Berlin, Germany), with the spectrum indicating the presence of carbon, oxygen, and Al.

BALF cytokine and chemokine measurement

The first cell-free BALF from 1 and 14 days post-exposure mice was utilized to analyze cytokine and chemokine protein levels as previously described (Mercer et al. 2013) with a V-Plex pro-inflammatory Panel (mouse) kit (Meso Scale Discovery, Gaithersburg, MD) using the manufacturer guidelines. Samples were run in duplicate. The following cytokine/chemokines were determined: interferon gamma (IFN-γ), interleukin-10 (IL-10), interleukin-12 (IL-12p70), interleukin-1 beta (IL-1β), interleukin-2 (IL-2), interleukin-4 (IL-4), interleukin-5 (IL-5), interleukin-6 (IL-6), neutrophil-activating protein 3 (KC/GRO), and tumor necrosis factor-alpha (TNFα).

Statistical analysis

Statistical comparisons for saline control, SSC, and silica-exposed groups across all concentrations were performed separately for each post-exposure time using analysis of variance (ANOVA). Since variance estimates were different across treatment groups, the ANOVA models were estimated employing an unequal variance method available from SAS PROC MIXED (Littell R.C. 2002). Similarly, comparisons across exposure times for each concentration were performed using unequal variance ANOVA. All statistical tests were two-tailed with the significance level set to 0.05.

Results

Material characterization

Qi, Echt, and Murata (2016) reported a d_{pg} of 1.05 μm and a σ_g of 1.78 for the airborne sawing SSC dusts, and an ATH content of 82.2% ± 4.1% in the respirable dust. For the present study, in order to confirm that the particle in the aspiration solution used to deliver to the lung was similar to real-time aerosol generated by SSC sawing, particles generated from the Qi, Echt, and Murata (2016) investigation were dispersed in saline, placed under vacuum and deposited onto polycarbonate filters, and imaged with FE-SEM. The SSC particle geometric d_{pg} was 1.16 μm, σ_g = 2.18, when dispersed in the saline employed for animal exposures (Figure 1). Taking into account dust density by using the Corian® board density obtained from measuring the mass and volume of multiple boards (1.57 g/cm^3) as well as the dust shape factor of 1.36 (quartz dust)(Hinds 2012), the sawing dusts in the saline have a number-based geometric mean aerodynamic diameter of 1.25 μm, which is close to that of the real-time SSC sawing dust (1.05 μm), indicating that our aspiration exposure distribution was similar to inhalation. It should be noted that the bimodal distribution observed in Figure 1 indicates a substantial population of particles smaller (approximately 0.6 μm) than the geometric mean of 1.16. These smaller particles may contribute to enhanced toxicity compared to a homogenous population of larger particles of the same composition (Nel et al. 2006). ICP analysis for metal elements found that 21% of SSC particulate was Al by mass, which corresponds with an ATH content of 61.7% (assuming all Al present in the sample was in the ATH form). The lower ATH content in these particles compared to that in the respirable dust (82.2%±4.1%) is due to the reported lower ATH content in larger dusts, which were not in the respirable fraction but collected in the Teflon filter cartridges. The specific surface area was 1.39 ± 0.01 m^2/g. When suspended in 10 mM saline and sonicated for 1 min, the hydrodynamic diameter was 347.5 ± 16.2, with a zeta potential of −40.4 ± 1.18 mV, indicating adequate dispersion. SEM/EDX analysis indicated

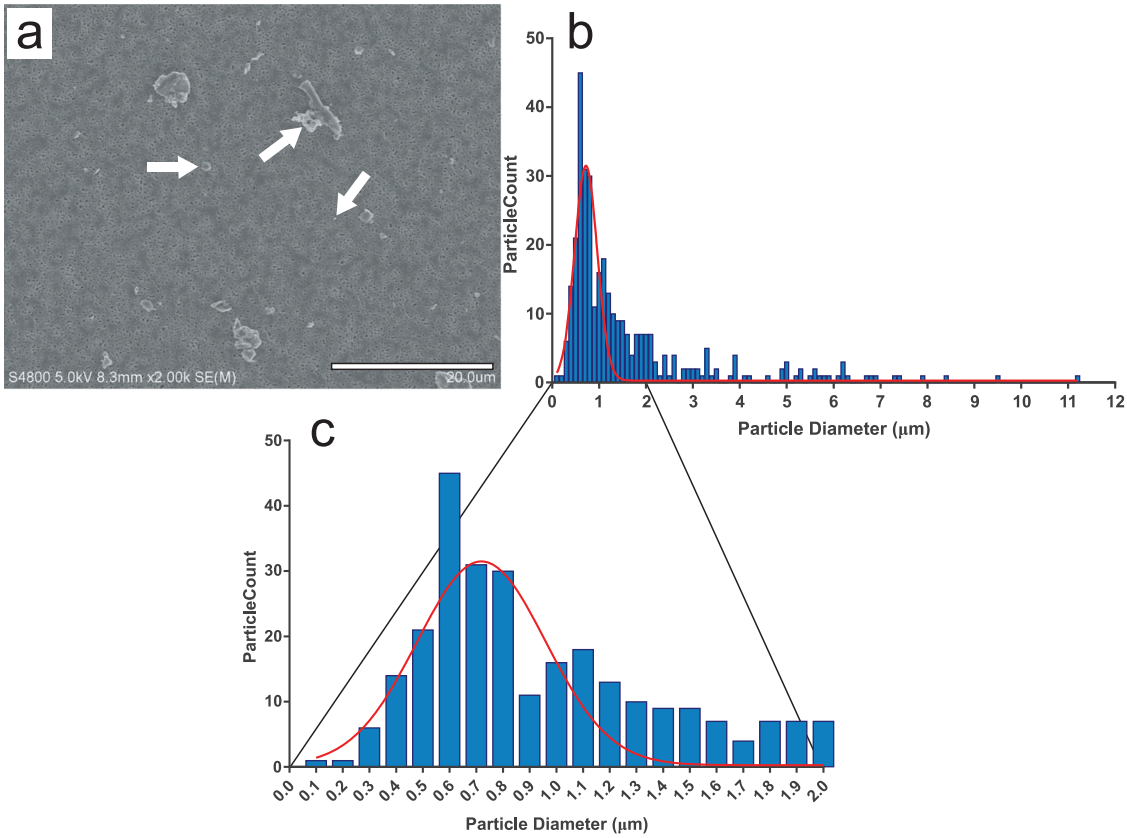

Figure 1. Particle Size Distribution. a) Electron micrograph of SSC particles deposited on polycarbonate filters following suspension in saline. Particle diameter was measured manually using ImageJ. b) Particle size distribution of SSC particles following suspension. Geometric mean particle diameter was 1.16 µm, σ_g = 2.18. C) Bimodal distribution of small particles showing a peak at 0.6 µm and 1.1 µm.

the presence of Al, oxygen, and carbon in particles deposited in the lung (Figure 2).

Pulmonary distribution of SSC particles

EDM analysis was used to investigate the deposition of SSC particles in lung sections. Figure 3 depicts representative enhanced dark-field images of lungs from the 1000 µg-exposed group at 1 day after exposure. As illustrated in Figure 3a, most particles were detected either in the lumen of terminal bronchioles or immediate proximal alveolar region. In addition, there was a diffuse component of the initial distribution consisting of singlets and small clusters distributed throughout the alveolar regions of the lungs (Figure 3b). Approximately half of this diffuse component was found phagocytized within alveolar macrophages and the remainder consisted of free particles located in the airspaces.

Comparisons of the distribution of SSC particles 14 days after aspiration for 1000, 250 and 62.5 µg doses are presented in Figure 4. Generally, particles were found concentrated in granulomas within the alveoli immediately proximal to the terminal bronchiole for all three dose groups. Particles in terminal bronchioles, as seen at day 1 post-exposure in the high dose, were infrequent in 14 day 1000 µg dose and absent in the 250 and 62.5 µg dose groups. The extent of the granulomatous region was dose-dependent. In contrast to terminal bronchioles, particles were persistent in the alveolar region over the 14 day post-exposure recovery period for all three exposure levels. Singlets and small clusters distributed throughout the more distal alveolar regions persisted in the 1000 µg dose group and were also present, at a proportionally lower concentration in the 250 and 62.5 µg dose groups at 14 days post-exposure. At 14 days post-exposure, the lung burden of Corian® was reduced from the 1 day post-exposure by 19%.

To summarize, at day 1 post-exposure, SSC particles were observed to be deposited in the terminal bronchioles and alveoli in all three exposure groups.

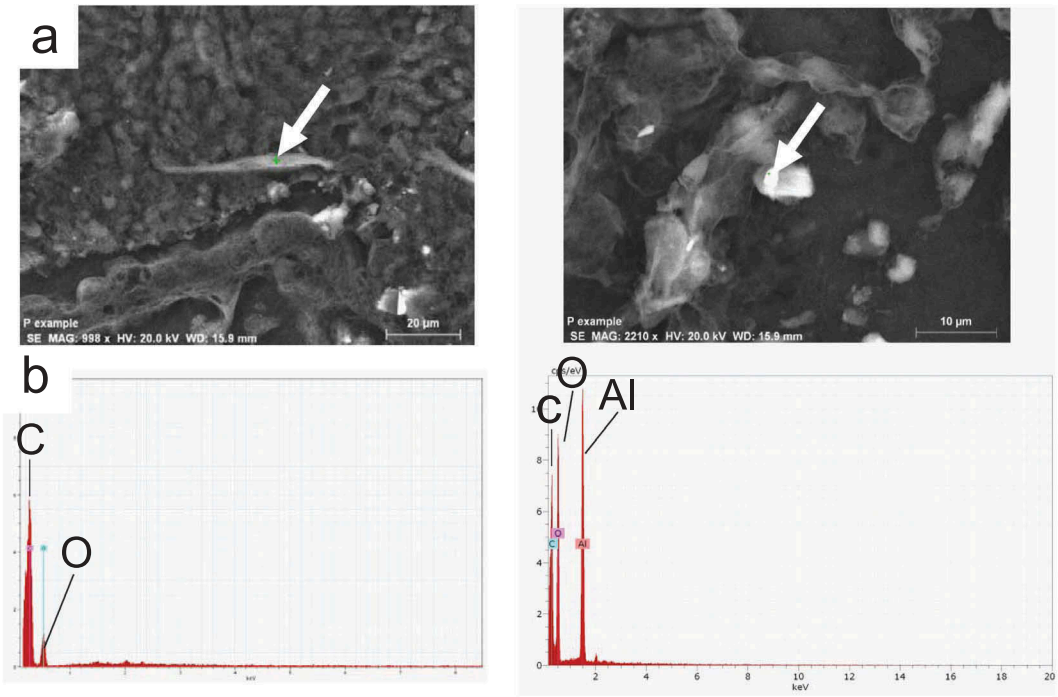

Figure 2. Organo-aluminum particles deposited in the lung. a) Electron micrographs of particles embedded in the lung. b) Corresponding EDX Spectra indicate the presence of carbon, oxygen, and aluminum.

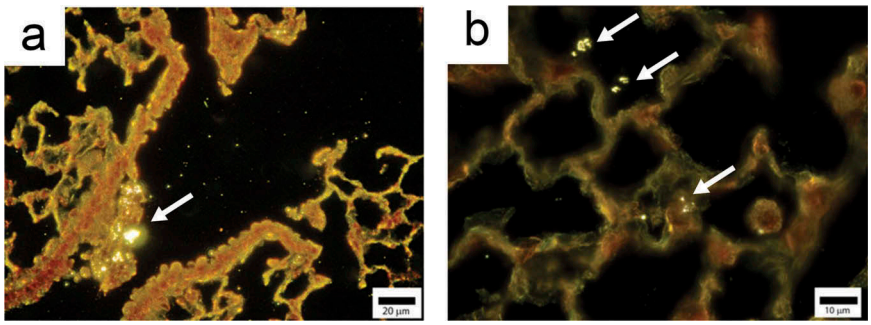

Figure 3. Enhanced darkfield micrographs of SSC deposition pattern in lungs at 1 day post-exposure to 1000 µg dose. a) Terminal bronchiole partially blocked with large particle mass in lumen. b) Higher magnification image of distal alveolar region which illustrates the frequent occurrence of singlet particles in the airspaces and phagocytized by alveolar macrophages throughout the lungs.

At day 14, particles were largely cleared from the terminal bronchioles in the 62.5 and 250 µg; however, a small number remained in the 1000 µg group. Most particles at day 14 were noted in alveolar granulomas for all three groups. These findings suggest incomplete clearance at this time point.

Body weight changes following SSC exposure

Immediately following SSC dosing, all SSC-exposed mice exhibited low movement, rounded backs, and puffed up fur, although breathing appeared unimpaired. Bodyweight was measured daily post-exposure as an indicator of stress and overall health. Body weight at post-exposure day 1, as % of pre-exposure baseline, was lower in the 1000 µg silica (−3.3 ± 0.69%), 1000 µg SSC (−10.4 ± 1.4%), 500 µg SSC (−5.6 ± 0.7%), and 250 µg (−1.6 ± 2%) SSC groups, compared to control (4.4 ± 0.5%) (Figure 5). On day 14, the SSC 250 µg (8 ± 0.62%), SSC 500 µg (6.7 ± 0.9%) and SSC 1000 µg (7.2 ± 0.7%) groups were still significantly lower than saline control (11.7 ± 1.3%), indicating a reduced growth rate in these groups.

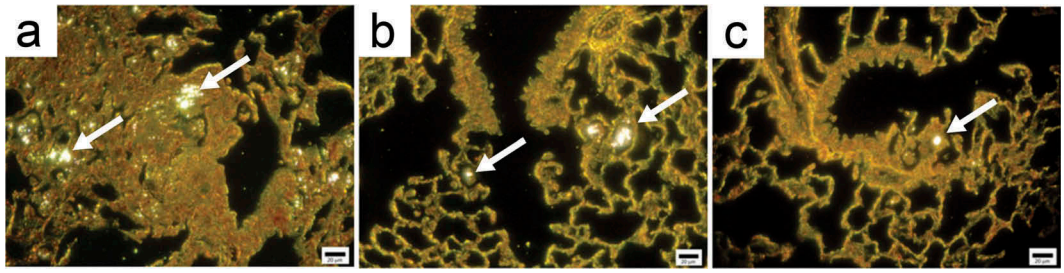

Figure 4. Comparative enhanced darkfield micrographs of SSC particle deposition pattern in lungs 14 days after aspiration with 1000 µg (A), 250 µg (B), and 62.5 µg C) doses. Figure 4a) Large, particle-rich granulomatous masses were frequently observed in the 1000 µg dose-exposed lungs at 14 days post-exposure in the alveolar region immediately proximal to the terminal bronchiole. The granulomatous masses in lungs exposed to either 250 or 62.5 µg doses (Figure 4b–C, respectively) were significantly smaller and less frequent than those found in the higher doses.

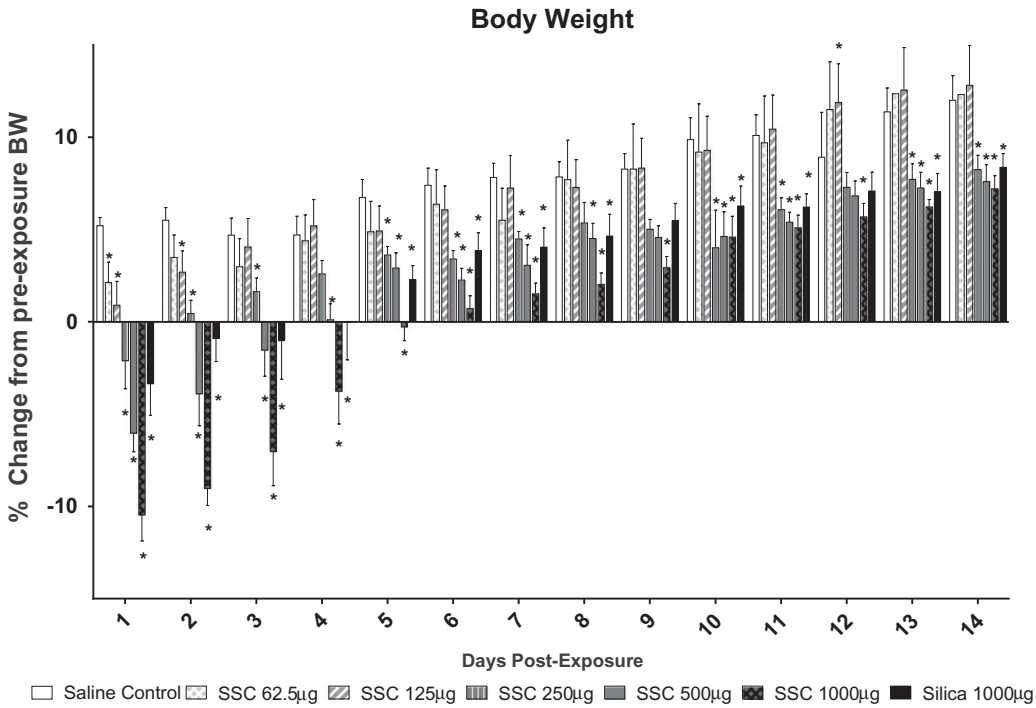

Figure 5. Body weights. As a percent of pre-exposure weight, body weights were significantly reduced at day 1 in the SSC 250, 500, and 1000 µg groups, as well as the Silica group. This reduction persisted until the end of the study in the 500 and 1000 µg SSC groups. * indicates a statistically significant difference from saline control, $p < .05$.

SSC-induced pulmonary histopathologic changes

At day 1 post-exposure, acute bronchiolitis and alveolitis were detected in lungs of all exposed mice at each dose tested (Figure 6). Cellular infiltrates were composed of variable numbers of viable and degenerate neutrophils that were centered at terminal bronchioles with extension into alveolar ducts and adjacent alveoli. The severity of this change was mild-to-moderate (mean severity score of 2.5) following high and intermediate dose exposures with a dose-dependent reduction in severity seen at the low (mean severity score of 1.5). Deposits of foreign material were frequently observed within foci of inflammation and within alveolar macrophages at this time point.

At 14 days following the intermediate and low-doses, resolution of acute inflammation with clearance of foreign material was found (Figure 7). At this time point, minimal lung pathology was detected, consisting of small clusters of macrophages located at terminal bronchioles or within alveoli. Small amounts of extracellular collagen were present within these foci of inflammation often in association with particle

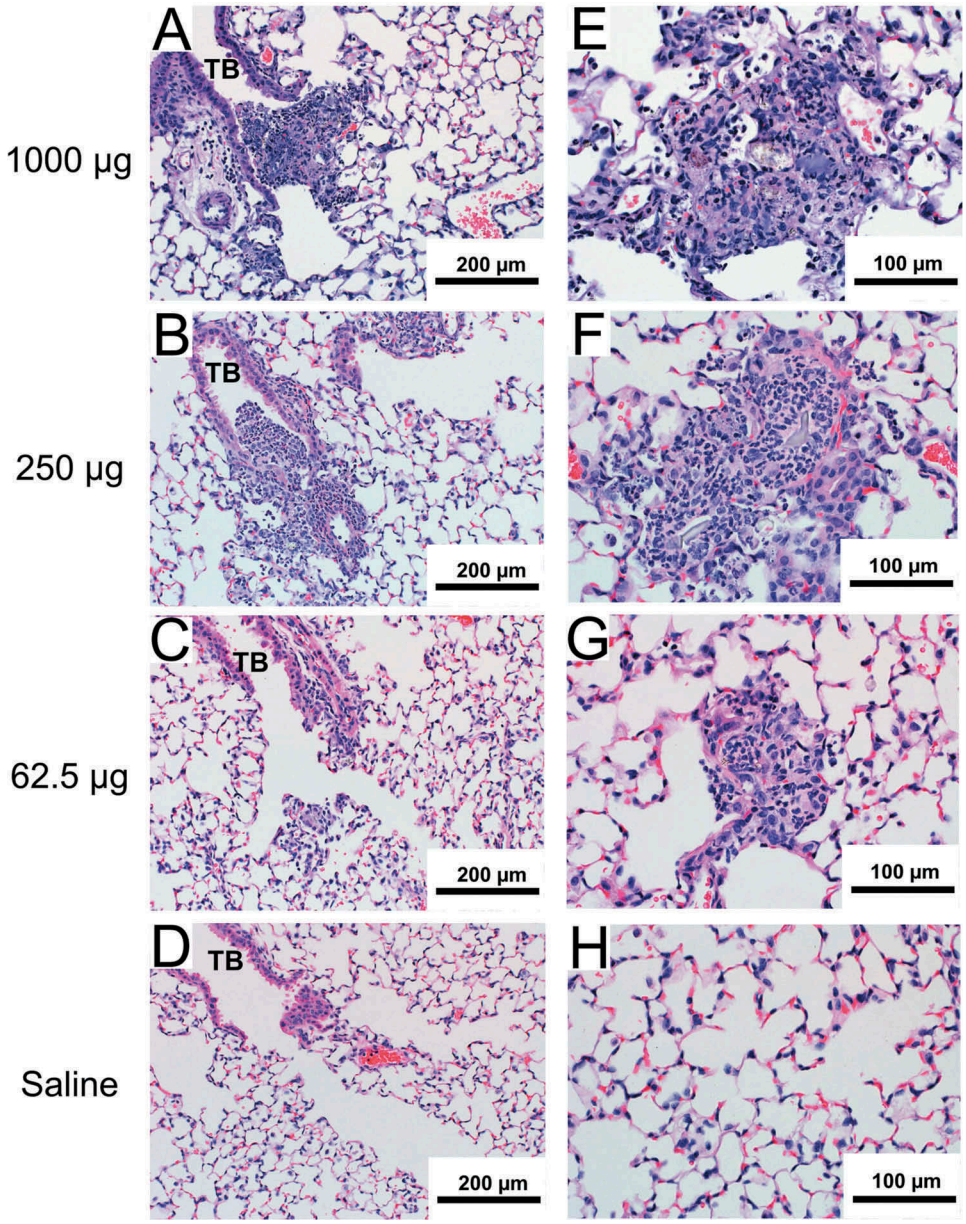

Figure 6. Representative photomicrographs of H&E stained lung sections from mice exposed to three different doses of SSC dust, and sacrificed at day 1 post-exposure. Neutrophilic inflammation is seen at terminal bronchioles (TB) (A, B, and C) and within alveoli (E, F, and G) at all doses, but the severity is reduced at the low (62.5 µg) dose. Normal lung anatomy is shown in saline-exposed lung for comparison (D and H).

deposits. These findings indicate that at the lower doses of SSC, there is particle clearance with the resolution of acute inflammation, whereas at 1000ug, particles are retained within the lung and there is a shift from acute neutrophilic inflammation to sustained granulomatous inflammation.

Pulmonary damage and inflammation

BALF was analyzed for lactate dehydrogenase activity and cell differentials from mice exposed to saline, 62.5, 125, 250, 500, and 1000 µg SSC, and 1000 µg silica (Figure 8). At day 1, BALF LDH was elevated in all exposure groups with the 500 and 1000 µg SSC groups exhibiting higher levels than silica, by day 14, only 500, 1000 µg SSC, and silica groups remained elevated. A significant PMN influx was noted at day one for 250 µg and above exposure groups, while at day 14, only 1000 SSC remained elevated. The eosinophil subset of PMNs was also increased at 250 µg and above exposure groups at day 1, while at day 14 both 1000 µg SSC and silica remained elevated. There were

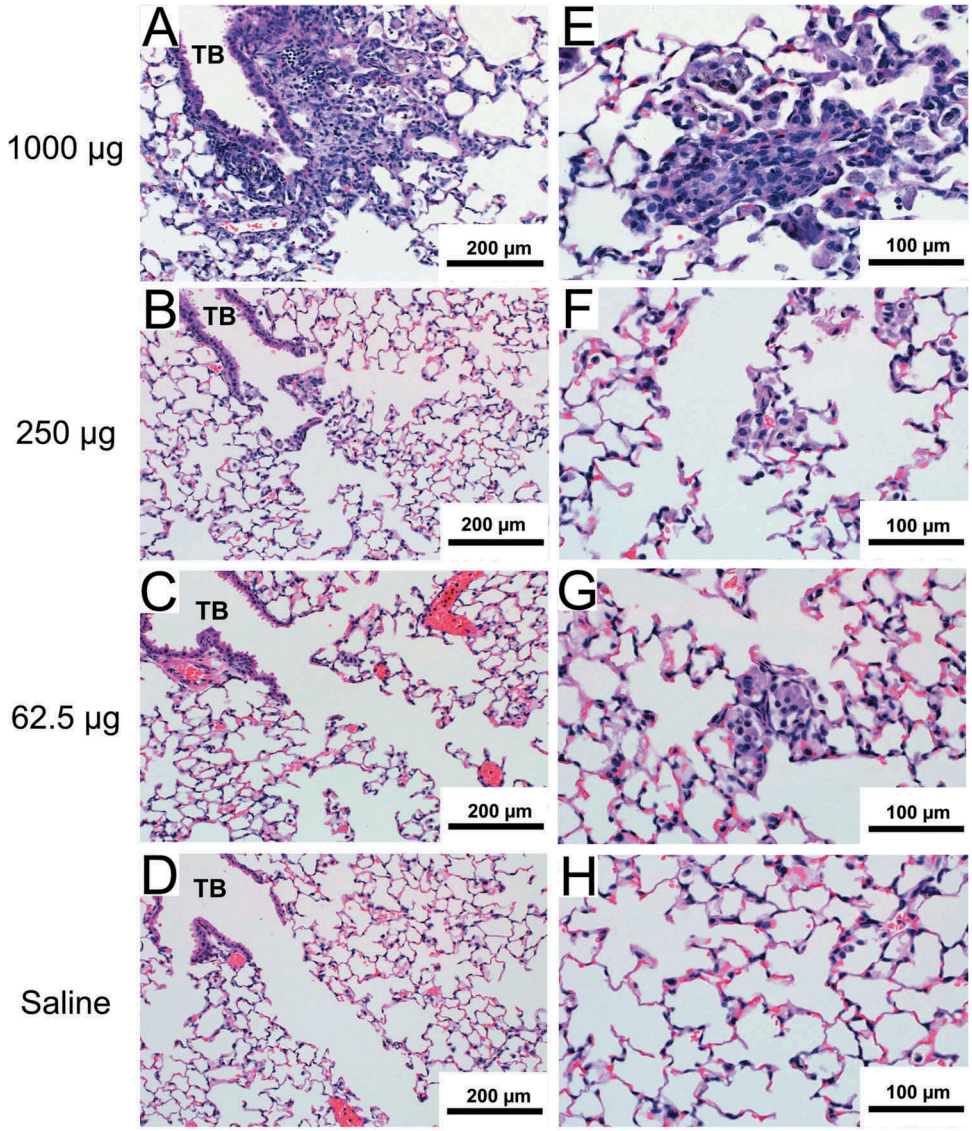

Figure 7. Representative photomicrographs of H&E stained lung sections from mice exposed to three different doses of SSC dust, and sacrificed at day 14 post-exposure. There is near complete resolution of the neutrophilic bronchiolitis seen at day 1 following the middle (250 µg) and low (62.5 µg) dose exposures (B and C) with only a few small clusters of macrophages present in the alveoli (F and G). With the high (1000 µg) dose exposure, granulomatous inflammation is seen at terminal bronchioles (TB) (A) and within alveoli (E). Normal lung anatomy is shown in saline-exposed lung for comparison (D and H).

no marked changes at day 1 in BALF macrophage count; however, a great number of macrophages were present in the 250 µg and higher exposure groups at day 14.

BALF was also analyzed for inflammatory cytokines. IL-1β, IL-2, IL-4, IL-5, IL-6, IL-12, KC/GRO, TNFα, and IFNγ levels were determined by MesoScale Discovery (Figure 9). At day 1, IL-4 and IL-5 were elevated in BALF for all exposure levels. IL1-β was enhanced at 125 µg and above, while TNFα was increased at 250 µg and above. IL-2 and IL-6 were elevated at 500 µg and higher doses. kC/GRO was enhanced only in the 500 µg SSC and silica exposure groups, while IL-12 was only increased in the highest exposure groups. At day 14, only TNFα and IFNγ were elevated at 1000 µg exposure levels.

Discussion

This study represents the first systematic investigation of the toxicological potential of emissions from SSC sawing. While this study was limited in scope due to short duration, our data suggest that exposure to SSC emissions elicits acute

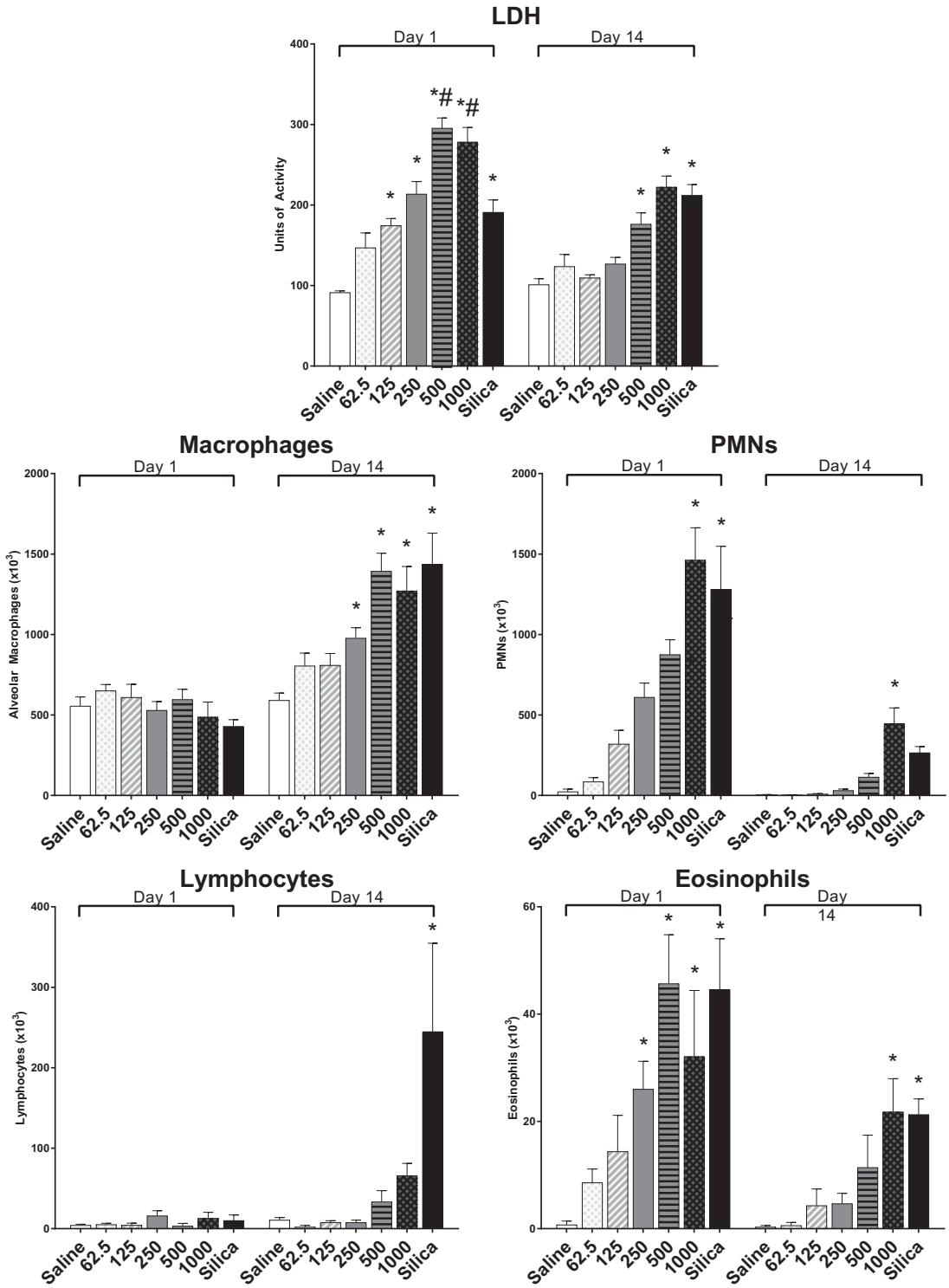

Figure 8. Pulmonary damage and inflammation. BALF was analyzed for lactate dehydrogenase activity and cell differentials from mice exposed to saline, 62.5, 125, 250, 500, and 1000 µg SSC, and 1000 µg silica. A) LDH, B) PMN, C) eosinophils, and D) alveolar macrophages were counted from each BALF Cytospin. Values are means ± standard errors. n = 7–10 mice per group. * represents significance ($p < .05$) between saline control and SSC or silica-exposed mice. # represents significance ($p < .05$) between SSC and silica groups.

inflammatory responses similar to silica particles. Silica was selected as a positive control as this substance is well known to produce acute lung inflammation and eventual fibrosis (Anlar et al. 2017; Lakatos et al. 2006; Lin et al. 2006; Scabilloni et al. 2005; Umbright et al. 2017).

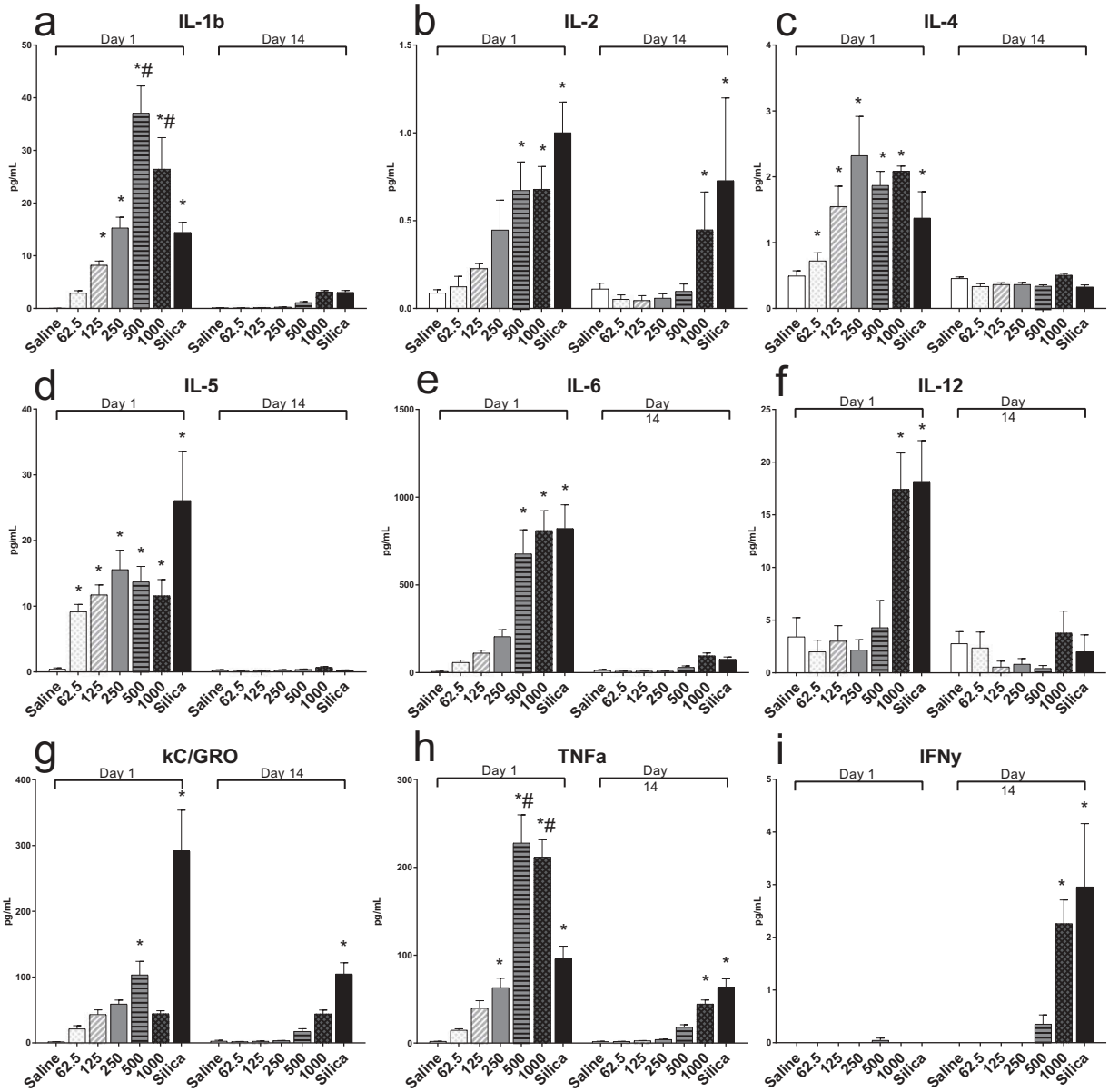

Figure 9. BALF Inflammatory cytokines. BALF was analyzed for inflammatory cytokines from mice exposed to saline, 62.5, 125, 250, 500, and 1000 µg SSC, and 1000 µg silica. A) IL-1β, B) IL-2, C) IL-4, D) IL-5, E) IL-6, F) IL-12, G) KC/GRO, H) TNFα, and I) IFNγ levels were determined by MesoScale Discovery. Values are mean ± standard error. n = 7–10 mice per group. * represents significance ($p < .05$) between saline control and SSC or silica-exposed mice. # represents significance ($p < .05$) between SSC and silica groups.

Our previous characterization of the airborne particle size distribution from sawing SSC indicated a mass-based geometric mean aerodynamic diameter of 4.19 µm, σ_g = 2.15, and a number-based geometric mean aerodynamic diameter of 1.05 µm, σ_g = 1.78. Thirty-two percent of the aerosol by mass was respirable (Qi, Echt, and Murata 2016). Because of the aspiration delivery method, it was important to confirm that particle size distribution was not markedly altered by the suspension of the SSC particles in saline. The number-based geometric mean aerodynamic diameter in suspension was similar (1.25 µm, σ_g = 2.18) to that reported by (Qi, Echt, and Murata 2016) for real-time SSC sawing dust. Minimal aggregation was observed suggesting an effective dispersion. One important consideration for this study is that due to aspiration delivery route, the entire fraction of airborne material (not only the respirable fraction) was potentially delivered to the

alveolar region. Unfortunately, it was not possible to generate a sufficient amount of respirable-only SSC particles to conduct this investigation. Future studies of pulmonary SSC toxicity need to consider delivery methods that closely replicate "real-world " exposures (e.g. inhalation of particles generated in real-time).

At 1 day post-dosing, alveolar deposition of SSC particles was found in all examined groups. Some clearance was observed over the following 13 days, but even at the lowest exposure, particles were detected within granulomatous masses in the alveolar region. Particle phagocytosis is negatively correlated with particle size (Oberdörster 2001), and particle-induced lung toxicity was associated with macrophage-derived inflammatory signals (Mantecca et al. 2009). Sustained presence of particles at 14 days post-exposure in all treated groups suggests that SSC dusts are not rapidly cleared from the alveolar space; however, this time point is too early to make definitive predictions regarding the long-term fate of these particles in the lung. The incomplete clearance noted in this study is congruous with other, longer-term, investigations of pulmonary exposure to aluminum oxide (Al_2O_3) particulates. Schlesinger et al. (2000) demonstrated that 19 weeks after a 20-week chronic (1 mg/kg/week) instillation of Al_2O_3 (MMAD = 1.2 μm), there was no marked difference in Al burden between 1 day post-exposure and 20 weeks post-exposure, indicating poor clearance. In rats exposed via inhalation to 0.4, 3, or 28 mg/m^3 in two 4-week (6 h/day, 5 days/week) exposures to Al_2O_3 particles (MMAD = 1.7 μm), particle half clearance duration was 42, 60 or 295 days, respectively. One of the principal challenges of the present study is assessing the toxicity of a mixed-exposure. There currently is no apparent information regarding lung burden and clearance rates with Al particles embedded in an organic matrix. Future investigations need to address SSC lung burden and clearance rates over an extended (>30 days) time period.

Animal body weights were significantly reduced from baseline in the higher SSC groups, and failed to attain the same growth rates noted in controls. There have been no apparent investigations of the relationship between ATH or PMMA exposure and body weight. However, pulmonary exposures to other particulates, including laser printer toner (Bai et al. 2010), and alumina-coated titanium dioxide (Warheit et al. 2005) particles were associated with decreases in body weight and growth. Weight loss is associated with animal stress and is a broad indicator of health and mortality in lab rodents (Wallace 1976). Evidence indicates that overall animal health and welfare was reduced in the 250, 500, or 1000 μg SSC and silica groups.

The rise in BALF inflammation-associated cytokines, but lack of change in BALF macrophage count at day 1, at first, appears to be incongruous, but may be due to a limitation of the bronchoalveolar lavage technique. Castranova et al. (1987) reported similar findings in guinea pigs and rats following inhalation exposure to cotton dust, despite enhanced superoxide release. Castranova et al. (1987) postulated that activation of macrophages by foreign material enabled them to adhere tightly to the epithelial surface, causing them to be more difficult to dislodge and thus collect *via* lavage. This hypothesis is supported by our enhanced darkfield morphology observations of widespread distribution of macrophages in the terminal bronchioles and alveoli at day 1 (Figure 3). It is also conceivable that some portion of the observed rise in inflammatory cytokines in day 1 BALF might be attributed to cell populations other than macrophages. Bronchiolar epithelial cells have been frequently noted as a source of pro-inflammatory cytokines following exposure to particulate matter (Boland et al. 1999; Huang, Hsu, and Chan 2003; Pelletier, Lavastre, and Girard 2002; Sakamoto et al. 2007).

Our histopathology findings demonstrated that SSC particles induced acute pulmonary inflammation and exhibited pro-fibrotic potential as evidenced by immune cell counts and cytokine levels in BALF. Following lung injury, neutrophils and macrophages are recruited to the injured tissue and release proinflammatory cytokines in a synergistic manner with the alveolar epithelium, including IL-1β, IL-4–5, TNFα, and MIP-2 (Tao and Kobzik 2002). The cytokines measured in the collected BALF provide information about the innate immune response induced by SSC exposure. Activated macrophages and lymphocytes, epithelial cells, and endothelial cells can produce TNFα, which might subsequently stimulate the

production of IL-1, IL-6, CXCL8, CCL2, PDGF, and TGF-β. Further, TNF-α may promote extracellular matrix degradation through the proliferation of fibroblasts (Agostini and Gurrieri 2006; Zhang et al. 1997). In mouse models, overexpression of TNFα induces leukocyte-mediated alveolitis, as well as the proliferation of desmin-containing fibroblasts, collagen fibers, and lymphocytes, resulting in a thickening of the alveolar walls (Miyazaki et al. 1995). Increased IL-1 results in pulmonary epithelium inflammation and tissue destruction, often with a subsequent production of pro-fibrotic cytokines, such as TGF (Kolb et al. 2001). Our data demonstrated that IL-1β and TNFα levels were elevated in SSC-exposed animals to a greater extent than silica-exposed controls. It should be noted that silica used in this study displays a different particle size distribution than SSC, which may partially explain the observed differences. The pattern of cytokine expression in BALF noted in this investigation is indicative of acute inflammation and a pro-fibrotic shift in lung physiology, although the limited time course in this study precludes making conclusions regarding chronic fibrotic potential.

As previously indicated by Chew, Nigam, and Sivakumaran (2016), an individual was diagnosed with terminal idiopathic interstitial fibrosis following several years of working with SSC. Unfortunately, it is not possible to determine the amount of SSC exposure in that case retrospectively. The wide dose range selected for this study was selected in order to elicit a continuum of responses, ranging from no to maximal effect. The dose range employed in this investigation has been related to a human occupational exposure based upon an estimated equivalent mass dosage to the human alveolar epithelium. While the higher SSC levels utilized were large in terms of typical mouse single exposures, and are possibly in the range associated with pulmonary overload (Oberdorster 1995) these amounts correlate to relatively low human worker equivalent exposure years. Further investigations are needed to evaluate the influence of chronic, repeated exposure to occupationally relevant quantities of SSC particulate.

The validity of exposure to SSC dusts by oropharyngeal aspiration vs. whole body inhalation is an area of sustained debate. Because SSC has yet to be investigated, no apparent information exists yet regarding the distribution of SSC particles during inhalation. It is possible, however, to make inferences regarding the equivalence between inhalation and aspiration using another material extensively characterized by our group: multi-walled carbon nanotubes (MWCNT). In these cases, the MWCNT was delivered in a similar mass-dose (40 μg suspended in 50 μl saline), utilizing the same aspiration technique (Mercer et al. 2010). One day after oropharyngeal aspiration exposure, 82% of MWCNT lung burden was distributed in the alveoli with the remainder found in the airways. In comparison, for mice which were exposed to MWCNT by whole-body inhalation, 84% and 16% of MWCNT lung burden was in the alveolar and airway regions, respectively, at 1 day post-exposure (Mercer et al. 2013). These findings indicated that oropharyngeal aspiration and whole body inhalation resulted in similar MWCNT distributions in the lung. Comparison of whole lung lavage PMN demonstrated that the responses to 10 μg MWCNT by oropharyngeal aspiration resembled those to whole body inhalation dose of 13 μg MWCNT (Porter et al. 2013). While the physical characteristics of MWCNT are different from SSC, data suggest that aspiration exposure may be a useful analogue to whole body inhalation for toxicology studies. Further inhalation studies are required to confirm the toxicity detected using aspiration exposure. It should also be noted that the particulate employed in this investigation was composed of all airborne particulate generated by sawing, not only the inhalable or respirable fractions. Aspiration, in this case, may have delivered normally non-respirable particles to the alveolar region in this case. This method of exposure would not contain any VOCs that may be generated during sawing. Future experiments need to address these considerations by using real-time generation and inhalation exposure.

While the potential toxicity of SSC particles is still under investigation, it is apparent that the individual components of SSC represent pulmonary hazards. Occupational pulmonary exposure to Al particles or welding fumes, typical forms of aluminum oxides, was associated with respiratory pathology (Gomes et al. 2014; Hull and Abraham 2002;

Krajnak et al. 2017). Exposure to aluminum oxides was correlated with impaired lung mechanics and an influx of PMN (Mazzoli-Rocha et al. 2010), pulmonary fibrosis (Hubbard et al. 2000; McLaughlin et al. 1962), asthma (Sjaheim et al. 2004), chronic bronchitis (Alessandri, Baretta, and Magarotto 1992) and granulomatosis (Chen et al. 1978). Several occupational exposures are commonly associated with Al-induced lung damage. These occupations include bauxite smelting (Wyatt and Riddell 1949), use of powdered Al in propellants (Dinman 1987), welding (Hull and Abraham 2002), and working with Al-containing abrasives (Miller et al. 1984; Shaver and Riddell 1947). Investigations of the pulmonary toxicity of ATH, the predominant form of Al contained in SSC, are limited. Intratracheal instillation of ATH was found to generate discrete lung lesions and collagenous fibrosis, progressing to development of firm fibrotic areas and eventual confluent masses at 180 days post-exposure (Stacy et al. 1959). Another major component of solid-surface composite materials is acrylate polymers. Manufacturing and fabricating products containing acrylate polymers using power tools may release ultrafine particles (diameters <100 nm) and VOC, which contain methyl methacrylate. (Reininghaus, Koestner, and Klimisch 1991). Inhalation of methyl methacrylate is associated with degeneration of olfactory epithelium at low exposures (15-200ppm) (Mainwaring et al. 2001; Reininghaus, Koestner, and Klimisch 1991), and bronchopneumonia, interstitial pneumonia, hemorrhage, atelectasis, edema, emphysema, and bronchial epithelial hyperplasia at high exposures (1000 ppm) (Aydin et al. 2002). The potential toxicity of these ingredients when combined in a heterogeneous mixture, as observed in SSC dusts, has yet to be determined.

Conclusions

The present study demonstrated that particulate emissions from sawing SSC are comprised primarily of Al and hydrocarbons. These findings represent the first attempt to characterize pulmonary toxicity of emissions released by sawing SSC, and suggest that there may be acute toxicity hazards associated with this exposure. The doses in which most severe effects were noted, 500 and 1000 μg, are large for a single bolus dose in mice; however, these doses represent equivalent amounts for a worker exposed to SSC at less than one-half of the current regulatory limits of 3.4 and 6.8 years, respectively. The relatively short post-exposure observation period used in this study (14 days) provided information regarding the acute inflammation and resolution in the immediate days following exposure. These preliminary results might help guide future investigations with this material, focusing on smaller, repeated exposures with a longer post-exposure observation period and *in vitro* mechanistic studies.

Authors' contributions

CQ, YQ, and JDS contributed to the study design and conception. JDS and JS performed the toxicological experiments. WKM performed particle size distribution experiments, prepared figures and drafted the manuscript. CQ performed particle generation and contributed to the manuscript. LAB performed tissue collection for histological examination. MSO performed histopathology and contributed to the manuscript. KS performed statistical analysis. RRM performed enhanced dark-field image analysis and contributed to the manuscript. SF performed electron microscopy. JS assisted with ABS, AKK, and LNB performed material characterization experiments and contributed to the manuscript.

Competing interests

The authors declare that they have no competing interests with respect to the research, authorship, and/or publication of this article.

Disclaimer

The findings and conclusions in this report are those of the authors and do not necessarily represent the official position of the National Institute for Occupational Safety and Health, Centers for Disease Control and Prevention.

Ethics approval

All procedures in the study comply with the ethical standards set forth by the Animal Welfare Act (enforced by the United States Department of Agriculture) and the Office of Laboratory Animal Welfare (OLAW). The studies were approved by the NIOSH Health Effects Laboratory Division (HELD) Institutional Animal Care and Use Committee within the Center for Disease Control.

Funding

Internal NIOSH funding.

References

Agostini, C., and C. Gurrieri. 2006. Chemokine/cytokine cocktail in idiopathic pulmonary fibrosis. *Proc Am Thorac Soc* 3:357–63. doi:10.1513/pats.200601-010TK.

Alessandri, M. V., L. Baretta, and G. Magarotto. 1992. Chronic bronchitis and respiratory function in those employed in primary aluminum production. *Med Lav* 83:445–50.

Anlar, H. G., M. Bacanli, S. İritaş, C. Bal, T. Kurt, E. Tutkun, O. H. Yilmaz, and N. Basaran. 2017. Effects of occupational silica exposure on oxidative stress and immune system parameters in ceramic workers in Turkey. *J Toxicol, Environ Health A* 80:688–96. doi:10.1080/15287394.2017.1286923.

Aydin, O., G. Attila, A. Dogan, M. V. Aydin, N. Canacankatan, and A. Kanik. 2002. The effects of methyl methacrylate on nasal cavity, lung, and antioxidant system (an experimental inhalation study). *Toxicol Pathol* 30:350–56. doi:10.1080/01926230252929927.

Bai, R., L. Zhang, Y. Liu, L. Meng, L. Wang, Y. Wu, W. Li, C. Ge, L. Le Guyader, and C. Chen. 2010. Pulmonary responses to printer toner particles in mice after intratracheal instillation. *Toxicol Lett* 199:288–300. doi:10.1016/j.toxlet.2010.09.011.

Boland, S., A. Baeza-Squiban, T. Fournier, O. Houcine, M. C. Gendron, M. Chévrier, G. Jouvenot, A. Coste, M. Aubier, and F. Marano. 1999. Diesel exhaust particles are taken up by human airway epithelial cells in vitro and alter cytokine production. *Am J Physiol Lung Cell Mol Physiol* 276:L604–L613. doi:10.1152/ajplung.1999.276.4.L604.

Castranova, V., V. A. Robinson, J. H. Tucker, D. Schwegler, D. A. Rose, D. S. DeLong, and D. G. Frazer. 1987. Time course of pulmonary response to inhalation of cotton dust in guinea pigs and rats. *Proc. Cotton Dust Res. Conf*, Dallas, Texas. 11: 3.

Chang, -C.-C., P.-S. Chen, and P.-S. Yang. 2015. Short-term effects of fine particulate air pollution on hospital admissions for cardiovascular diseases: A case-crossover study in a tropical city. *J Toxicol, Environ Health Part A* 78:267–77. doi:10.1080/15287394.2014.960044.

Chen, W. J., R. J. Monnat Jr., M. Chen, and N. K. Mottet. 1978. Aluminum induced pulmonary granulomatosis. *Human Pathol* 9:705–11. doi:10.1016/S0046-8177(78)80053-7.

Chew, R., S. Nigam, and P. Sivakumaran. 2016. Alveolar proteinosis associated with aluminium dust inhalation. *Occup. Med. (Lond.)* 66:492–94. doi:10.1093/occmed/kqw049.

Corian® Solid Surface Product Overview. 2018. Wilmington, DE: Corian Design.

Dinman, B. D. 1987. Aluminum in the lung: The pyropowder conundrum. *J Occup Med* 29:869–76.

Galer, D. M., H. W. Leung, R. G. Sussman, and R. J. Trzos. 1992. Scientific and practical considerations for the development of occupational exposure limits (OELs) for chemical substances. *Regul Toxicol Pharmacol* 15:291–306.

Gannon, P., and R. W. Rickard. 2014. Pulmonary fibrosis associated with aluminum trihydrate (Corian) dust. *N Engl J Med* 370:2156–57. doi:10.1056/NEJMc1404786.

Ghio, A. J., M. S. Carraway, and M. C. Madden. 2012. Composition of air pollution particles and oxidative stress in cells, tissues, and living systems. *J Toxicol, Environ Health B* 15:1–21. doi:10.1080/10937404.2012.632359.

Gomes, J. F., R. M. Miranda, T. J. Santos, and P. A. Carvalho. 2014. Emission of nanoparticles during friction stir welding (FSW) of aluminium alloys. *J Toxicol, Environ Health A* 77:924–30. doi:10.1080/15287394.2014.911132.

Hinds, W. C. 2012. *aerosol technology: properties, behavior, and measurement of airborne particles*. Hoboken, NJ: Wiley.

Huang, S. L., M. K. Hsu, and C. C. Chan. 2003. Effects of submicrometer particle compositions on cytokine production and lipid peroxidation of human bronchial epithelial cells. *Environ. Health Perspect.* 111:478–82. doi:10.1289/ehp.5519.

Huang, Y.-C. T., E. D. Karoly, L. A. Dailey, M. T. Schmitt, R. Silbajoris, D. W. Graff, and R. B. Devlin. 2011. Comparison of gene expression profiles induced by coarse, fine, and ultrafine particulate matter. *J Toxicol, Environ Health A* 74:296–312. doi:10.1080/15287394.2010.516238.

Hubbard, R., M. Cooper, M. Antoniak, A. Venn, S. Khan, I. Johnston, S. Lewis, and J. Britton. 2000. Risk of cryptogenic fibrosing alveolitis in metal workers. *Lancet* 355:466–67. doi:10.1016/S0140-6736(00)82017-6.

Hull, M. J., and J. L. Abraham. 2002. Aluminum welding fume-induced pneumoconiosis. *Human Pathol* 33:819–25. doi:10.1053/hupa.2002.125382.

Kolb, M., P. J. Margetts, D. C. Anthony, F. Pitossi, and J. Gauldie. 2001. Transient expression of IL-1beta induces acute lung injury and chronic repair leading to pulmonary fibrosis. *J Clin Invest* 107:1529–36. doi:10.1172/JCI12568.

Krajnak, K., K. Sriram, C. Johnson, J. R. Roberts, R. Mercer, G. R. Miller, O. Wirth, and J. M. Antonini. 2017. Effects of pulmonary exposure to chemically-distinct welding fumes on neuroendocrine markers of toxicity. *J Toxicol, Environ Health A* 80:301–14. doi:10.1080/15287394.2017.1318324.

Lakatos, H. F., H. A. Burgess, T. H. Thatcher, M. R. Redonnet, E. Hernady, J. P. Williams, and P. J. Sime. 2006. Oropharyngeal aspiration of a silica suspension produces a superior model of silicosis in the mouse when compared to intratracheal instillation. *Exp Lung Res* 32:181–99. doi:10.1080/01902140600817465.

Lin, W., Y. W. Huang, X. D. Zhou, and Y. Ma. 2006. In vitro toxicity of silica nanoparticles in human lung cancer cells. *Toxicol Appl Pharmacol* 217:252–59. doi:10.1016/j.taap.2006.10.004.

Ma, J., R. R. Mercer, M. Barger, D. Schwegler-Berry, J. M. Cohen, P. Demokritou, and V. Castranova. 2015. Effects of amorphous silica coating on cerium oxide nanoparticles induced pulmonary responses. *Toxicol Appl Pharmacol* 288:63–73. doi:10.1016/j.taap.2015.07.012.

Mainwaring, G., J. R. Foster, V. Lund, and T. Green. 2001. Methyl methacrylate toxicity in rat nasal epithelium: Studies of the mechanism of action and comparisons between species. *Toxicology* 158:109–18.

Mann, P. C., J. Vahle, C. M. Keenan, J. F. Baker, A. E. Bradley, D. G. Goodman, T. Harada, R. Herbert, W. Kaufmann, R. Kellner, et al. 2012. International harmonization of toxicologic pathology nomenclature: An overview and review of basic principles. *Toxicol Pathol* 40 (4 Suppl):7s–13s. doi:10.1177/0192623312438738.

Mantecca, P., G. Sancini, E. Moschini, F. Farina, M. Gualtieri, A. Rohr, G. Miserocchi, P. Palestini, and M. Camatini. 2009. Lung toxicity induced by intratracheal instillation of size-fractionated tire particles. *Toxicol Lett* 189:206–14. doi:10.1016/j.toxlet.2009.05.023.

Mazzoli-Rocha, F., A. N. Dos Santos, S. Fernandes, V. M. Ferreira Normando, O. Malm, P. H. Nascimento Saldiva, D. L. Wanderley Picanço-Diniz, D. S. Faffe, and W. A. Zin. 2010. Pulmonary function and histological impairment in mice after acute exposure to aluminum dust. *Inhal Toxicol* 22:861–67.

McKeever, R., J. Okaneku, and G. S. LaSala. 2014. More on pulmonary fibrosis associated with aluminum trihydrate (Corian) dust. *N Engl J Med* 371:973. doi:10.1056/NEJMoa1410490.

McKinney, W., M. Jackson, T. M. Sager, J. S. Reynolds, B. T. Chen, A. Afshari, K. Krajnak, S. Waugh, C. Johnson, R. R. Mercer, et al. 2012. Pulmonary and cardiovascular responses of rats to inhalation of a commercial antimicrobial spray containing titanium dioxide nanoparticles. *Inhal Toxicol* 24:447–57. doi:10.3109/08958378.2012.685111.

McLaughlin, A. I. G., G. Kazantzis, E. King, D. Teare, R. J. Porter, and R. Owen. 1962. Pulmonary fibrosis and encephalopathy associated with the inhalation of aluminium dust. *Br J Ind Med* 19:253–63. doi:10.1136/oem.19.4.253.

Mercer, R. R., A. F. Hubbs, J. F. Scabilloni, L. Wang, L. A. Battelli, D. Schwegler-Berry, V. Castranova, and D. W. Porter. 2010. Distribution and persistence of pleural penetrations by multi-walled carbon nanotubes. *Part Fibre Toxicol* 7:28. doi:10.1186/1743-8977-7-28.

Mercer, R. R., A. F. Hubbs, J. F. Scabilloni, L. Wang, L. A. Battelli, S. Friend, V. Castranova, and D. W. Porter. 2011. Pulmonary fibrotic response to aspiration of multi-walled carbon nanotubes. *Part Fibre Toxicol* 8:21. doi:10.1186/1743-8977-8-21.

Mercer, R. R., J. F. Scabilloni, A. F. Hubbs, L. A. Battelli, W. McKinney, S. Friend, M. G. Wolfarth, M. Andrew, V. Castranova, and D. W. Porter. 2013. Distribution and fibrotic response following inhalation exposure to multi-walled carbon nanotubes. *Part Fibre Toxicol* 10:33. doi:10.1186/1743-8977-10-56.

Mercer, R. R., J. F. Scabilloni, L. Wang, L. A. Battelli, J. M. Antonini, J. R. Roberts, Y. Qian, J. D. Sisler, V. Castranova, D. W. Porter, et al. 2017. The fate of inhaled nanoparticles: Detection and measurement by enhanced dark-field microscopy. *Toxicol Pathol*46:28–46 192623317732321.

Miller, R. R., A. M. Churg, M. Hutcheon, and S. Lam. 1984. Pulmonary alveolar proteinosis and aluminum dust exposure. *Am Rev Resp Dis* 130:312–15. doi:10.1164/arrd.1984.130.2.312.

Miyazaki, Y., K. Araki, C. Vesin, I. Garcia, Y. Kapanci, J. A. Whitsett, P. F. Piguet, and P. Vassalli. 1995. Expression of a tumor necrosis factor-alpha transgene in murine lung causes lymphocytic and fibrosing alveolitis. A mouse model of progressive pulmonary fibrosis. *J Clin Invest* 96:250–59. doi:10.1172/JCI118029.

Nel, A., T. Xia, L. Mädler, and N. Li. 2006. Toxic potential of materials at the nanolevel. *Science* 311:622–27. doi:10.1126/science.1114397.

NIOSH. 2003. *Elements by ICP. NIOSH manual of analytical methods*. Washington, DC: National Institute of Occupational Safety and Health.

Oberdorster, G. 1995. Lung particle overload: Implications for occupational exposures to particles. *Regul Toxicol Pharmacol* 21:123–35. doi:10.1006/rtph.1995.1017.

Oberdorster, G. 2001. Pulmonary effects of inhaled ultrafine particles. *Int Arch Occup Environ Health* 74:1–8.

Pelletier, M., V. Lavastre, and D. Girard. 2002. Activation of human epithelial lung A549 cells by the pollutant sodium sulfite: Enhancement of neutrophil adhesion. *Toxicol Sci* 69:210–16. doi:10.1093/toxsci/69.1.210.

Phalen, R. F. 1984. Basic morphology and physiology of the respiratory tract. *Inhal Stud Found Tech* 33–75.

Porter, D. W., A. F. Hubbs, B. T. Chen, W. McKinney, R. R. Mercer, M. G. Wolfarth, L. Battelli, N. Wu, K. Sriram, S. Leonard, et al. 2013. Acute pulmonary dose-responses to inhaled multi-walled carbon nanotubes. *Nanotoxicology* 7:1179–94. doi:10.3109/17435390.2012.719649.

Qi, C., A. Echt, and T. K. Murata. 2016. Characterizing dust from cutting Corian(R), a solid-surface composite material, in a laboratory testing system. *Ann Occup Hyg* 60:638–42. doi:10.1093/annhyg/mew005.

Raghu, G., B. F. Collins, D. Xia, R. Schmidt, and J. L. Abraham. 2014. Pulmonary fibrosis associated with aluminum trihydrate (Corian) dust. *N Engl J Med* 370:2154215–16.

Reininghaus, W., A. Koestner, and H. J. Klimisch. 1991. Chronic toxicity and oncogenicity of inhaled methyl acrylate and n-butyl acrylate in Sprague-Dawley rats. *Food Chem Toxicol* 29:329–39.

Renwick, L. C., K. Donaldson, and A. Clouter. 2001. Impairment of alveolar macrophage phagocytosis by ultrafine particles. *Toxicol Appl Pharm* 172:119–127. doi:.

Sakamoto, N., S. Hayashi, J. Gosselink, H. Ishii, Y. Ishimatsu, H. Mukae, J. C. Hogg, and S. F. van Eeden. 2007. Calcium dependent and independent cytokine synthesis by air pollution particle-exposed human bronchial epithelial cells. *Toxicol Appl Pharmacol* 225:134–41. doi:10.1016/j.taap.2007.07.006.

Scabilloni, J. F., L. Wang, J. M. Antonini, J. R. Roberts, V. Castranova, and R. R. Mercer. 2005. Matrix metalloproteinase induction in fibrosis and fibrotic nodule formation due to silica inhalation. *Am J. Physiol Lung Cell Mol Physiol* 288:L709–L717. doi:10.1152/ajplung.00034.2004.

Schlesinger, R. B., C. A. Snyder, C. L. Chi, J. E. Gorczynski, and M. Menache. 2000. Clearance and translocation of aluminum oxide (alumina) from the lungs. *Inhal Toxicol* 12:927–39. doi:10.1080/08958370050137996.

Schwarz, Y., S. Kivity, A. Fischbein, J. L. Abraham, E. Fireman, S. Moshe, Y. Dannon, M. Topilsky, and J. Greif. 1998. Evaluation of workers exposed to dust containing hard metals and aluminum oxide. *Am J Ind Med* 34:177–82.

Shackelford, C., G. Long, J. Wolf, C. Okerberg, and R. Herbert. 2002. Qualitative and quantitative analysis of nonneoplastic lesions in toxicology studies. *Toxicol Pathol* 30:93–96. doi:10.1080/01926230252824761.

Shaver, C. G., and A. R. Riddell. 1947. Lung changes associated with the manufacture of alumina abrasives. *J Ind Hyg Toxicol* 29:145–57.

Sjaheim, T., T. S. Halstensen, M. B. Lund, O. Bjortuft, P. A. Drablos, D. Malterud, and J. Kongerud. 2004. Airway inflammation in aluminium potroom asthma. *Occup Environ Med* 61:779–85. doi:10.1136/oem.2003.011627.

Stacy, B. D., E. J. King, C. V. Harrison, G. Nagelschmidt, and S. Nelson. 1959. Tissue changes in rats' lungs caused by hydroxides, oxides and phosphates of aluminium and iron. *J Pathol Bacteriol* 77:417–26.

Stone, K. C., R. R. Mercer, P. Gehr, B. Stockstill, and J. D. Crapo. 1992. Allometric relationships of cell numbers and size in the mammalian lung. *Am J Respir Cell Mol Bio* 6:235–43. doi:10.1165/ajrcmb/6.2.235.

Tao, F., and L. Kobzik. 2002. Lung macrophage–epithelial cell interactions amplify particle-mediated cytokine release. *Am J Respir Cell Mol Biol* 26:499–505. doi:10.1165/ajrcmb.26.4.4749.

Umbright, C., R. Sellamuthu, J. R. Roberts, S.-R. Young, D. Richardson, D. Schwegler-Berry, W. McKinney, B. Chen, J. K. Gu, M. Kashon, et al. 2017. Pulmonary toxicity and global gene expression changes in response to sub-chronic inhalation exposure to crystalline silica in rats. *J Toxicol, Environ Health A* 80:1349–68. doi:10.1080/15287394.2017.1384773.

Unwin, J., M. R. Coldwell, C. Keen, and J. J. McAlinden. 2013. Airborne emissions of carcinogens and respiratory sensitizers during thermal processing of plastics. *Ann Occup Hyg* 57:399–406. doi:10.1093/annhyg/mes078.

Wallace, M. E. 1976. Effects of stress due to deprivation and transport in different genotypes of house mouse. *Lab Animal* 10:335–47. doi:10.1258/002367776781035260.

Warheit, D. B., W. J. Brock, K. P. Lee, T. R. Webb, and K. L. Reed. 2005. Comparative pulmonary toxicity inhalation and instillation studies with different TiO2 particle formulations: Impact of surface treatments on particle toxicity. *Toxicol Sci* 88:514–24. doi:10.1093/toxsci/kfi331.

Wyatt, J. P., and A. C. R. Riddell. 1949. The morphology of bauxite-fume pneumoconiosis. *Am J Pathol* 25:447–65.

Zhang, K., M. Gharaee-Kermani, B. McGarry, D. Remick, and S. H. Phan. 1997. TNF-alpha-mediated lung cytokine networking and eosinophil recruitment in pulmonary fibrosis. *J Immunol* 158:954–59.